Tribology and Materials
Vol. 1, No. 2, 2022, pp. 61-69

ISSN 2812-9717
https://doi.org/10.46793/tribomat.2022.008

Gas metal arc welding of metal-polymer-metal sheets

Sebastian BALOS, Miroslav DRAMICANIN, Petar JANJATOVIC *

University of Novi Sad, Faculty of Technical Sciences, Novi Sad, Serbia
*Corresponding author: janjatovic@uns.ac.rs

Keywords
GMAW welding
metal-polymer-metal sheets
polymer layer loss

History
Received: 20-04-2022
Revised: 23-05-2022
Accepted: 09-06-2022

Abstract

Metal-polymer-metal (MPM) sheets are sandwich panels used for housings of large industrial electric motors and generators, vehicle body panels, flooring, various bulkheads, wheel arching, engine and gearbox shielding, etc. Their main advantage over classic steel panels in form of plates is their acoustic dampening properties. Joining of such plating is challenging because the polymer interlayer evaporates and the resulting fumes may cause the plates to deform. In this paper, GMAW welding was used to join metal-polymer-metal sheets, with a square butt joint, single V butt joint combined in one sheet, as well as welding in one pass per side and in multiple bead segments. C1 (CO_2) and M21 (Ar + 18 % CO_2) shielding gases were used. Tensile, bending and hardness tests were performed, macro and microstructures were tested and the evaporation, melting and cross-linking distances were recorded. It was shown that contrary to the recent tendency of using M21 shielding gas for GMAW welding, C1 proved to offer superior tensile and bending properties of the joint. From the point of view of simplicity and productivity, a square butt joint proved to be optimal.

1. Introduction

Innovative solutions for common engineering problems became crucial for providing both increased effectiveness of products and decreased cost. One special approach is the adoption of multipurpose materials, however, their fabrication and processing, most particularly their joining represent a considerable challenge. A typical multipurpose material is metal-polymer-metal (MPM) sheets consisting of three layers, a polymer layer between two cold rolled steel sheets [1-3]. MPM sheets are used for encasing large industrial electric motors and electric generators, vehicle body panels, flooring, various bulkheads, wheel arching, engine and gearbox shielding, battery carriers and crash boxes [4-6]. They provide the structural role for transportation, acting as a casing, but also provide an acoustic insulating role, dampening the sound generated by operating motors and generators. Steel provides the structural strength, while the polymer interlayer provides a sound dampening role. Sound dampening is essential for a low environmental impact of the encased device. The fabrication, forming and cutting of MPM sheets is simple, not time-consuming and cheap, however, their joining can represent a considerable challenge. As the main joining technology today is welding, the most severe obstacle is the large discrepancy between the melting point of steel and polymer [7,8]. Furthermore, the burning and evaporating point of polymers is lower than the melting point of steel. That means, when the common arc welding processes are used, when temperatures of the order of 4000 °C are developed and steel temperature is well above its melting point, the polymer interlayer evaporates, developing relatively large quantities of fumes. These fumes can cause distortion, that is, the plastic deformation in form of separation of steel sheets, which can compromise aesthetics, strength and sound dampening properties. Therefore, the most important aim during welding of MPM sheets, besides achieving a high-quality joint is to preserve the visco-elastic layer as much as possible. Welding techniques that are commonly used for MPM sheet

joining are spot and seam resistance welding, gas metal arc welding (GMAW) and GTAW (gas tungsten arc welding). Of these, the most common is GMAW, due to relatively cheap equipment and relatively high welding speed [9,10].

The aim of this study is to optimise the GMAW welding technology to obtain acceptable butt welds between MPM sheets, with sufficient productivity and to maintain the maximum depth of the polymer layer.

2. Experimental

MPM sheets used in this work consisted of two steel plates, 3 mm thick each. Between them was a layer of vinyl copolymer monomer based on acrylates, approximately 0.05 mm thick, bonding the two steel sheets. Chemical composition was determined by ARL-3460 optical emission spectrometer and LECO CS-244 infra-red (IR) spectrometer. The obtained chemical composition of steel sheets, as well as the equivalent carbon content (C_{EKV}), is shown in Table 1. The C_{EKV} was calculated in accordance with Equation (1) [11]:

$$C_{EKV} = C + \frac{Mn}{6} + \frac{Cr + Mo + V}{5} + \frac{Ni + Cu}{15}. \quad (1)$$

The C_{EKV} value of 0.074 is relatively low, indicating that this type of steel is readily weldable and does not demand the application of pre-heating or post-welding heat treatment [12]. Mechanical properties were tested by the application of VEB ZDM 5/91 tensile testing machine: *Re* = 175 MPa; *Rm* = 276 MPa; *A* = 40 %.

For the purpose of experimental work, MPM sheets were cut to the following dimensions 250 × 200 mm, which was deemed to be sufficient to allow effective confinement for evaporating gases from the polymer layer and, at the same time, large enough for macro, tensile and bend specimens.

These sheets were joined by GMAW along the longer side of the rectangle (250 mm side), by using an EWM Vega 500 device and by using Böhler EMK6 solid welding wire with typical chemical composition as follows: 0.08 % C, 0.9 % Si, 1.45 % Mn and weld metal mechanical properties as follows: *Re* ≥ 440 MPa, *Rm* ≥ 560 MPa and *A* ≥ 20 % [13]. Different welding parameters were applied, the most important being weld types (Fig. 1). Four butt-weld types were used: an open square butt joint with a 1 mm gap, a combined open square butt joint on a top sheet and a single V butt joint on the bottom sheet, welding in one pass on each side and welding in multiple bead segments on each side for each weld type (Fig. 1). When a square butt joint and an inverted V in the bottom were used, the first pass was done in the square half of the section, enabling the polymer to evaporate and escape through the V-shaped tunnel on the other side. All specimens (with different butt-weld types) were welded manually as described in Figure 1, with parameters given in Table 2.

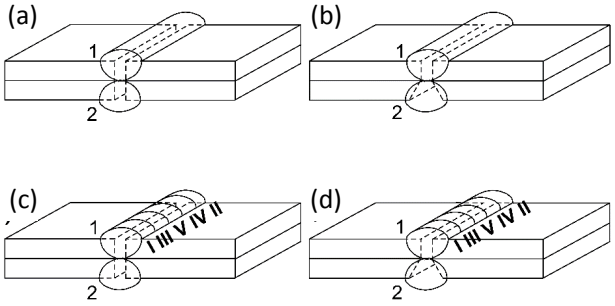

Figure 1. Butt welds: (a) specimen 1 and 5, (b) specimen 2 and 6, (c) specimen 3 and 7 and (d) specimen 4 and 8

To evaluate the weld properties, macro sections were taken, microstructure was explored, as well as mechanical properties were tested. Tensile and bend tests were done on a universal testing machine VEB ZDM 5/91, using three specimens per weld joint type (according to standard EN ISO 6892-1:2019). A 24 mm diameter pin was used for bending, with the distance between the supports of 36.5 mm and a maximum bending angle of 180°, according to standard EN ISO 5173:2010. Two specimens were bent over each side. Mechanical testing was done with welded MPM sheets, with polymer layer in unchanged condition after welding.

Macro and microstructures were evaluated after a standard metallographic preparation consisting of cutting, grinding, polishing and etching with 3 % nital solution (3 % nitric acid HNO_3 in alcohol). Hardness was measured on VEB HPO-250 Vickers testing machine with a loading of 10 kg in the pattern corresponding to 3 mm steel sheets, through base material (BM), heat affected zone (HAZ), weld metal (WM), HAZ and BM, with three indentations in each layer, as shown in Figure 2 (according to standard EN ISO 6507-1:2018). Also, the effect of welding in the polymer interlayer was evaluated by measuring several characteristic distances from the sheet edge that is welded, after separating two steel sheets. The characteristic distances correspond to the

Table 1. Chemical composition of steel sheets (wt. %) and C_{EKV}

C	Si	Mn	S	Cr	P	Al	Cu	Ni	Fe	C_{EKV}
0.03	0.01	0.187	0.01	0.05	0.01	0.04	0.018	0.023	balance	0.074

Table 2. Welding parameters

Figure 1	Specimen	Types of butt weld	Welding technique	Welding current, A	Welding speed, cm/min	Electrode inclination, °	Specimen and shielding gas	Shielding gas flow, l/min
(a)	1 and 5	square butt joint	welding in one pass on each side	150 (DC+)	42	60	1 – C1 5 – M21	12
(b)	2 and 6						2 – C1 6 – M21	
(c)	3 and 7	square butt joint on one sheet and V on the other sheet	welding in multiple bead segments on each side		14		3 – C1 7 – M21	
(d)	4 and 8						4 – C1 8 – M21	

evaporated, degraded and cross-linked polymer. Chemical compositions of weld metal and heat affected zones were determined by ARL-3460 optical emission spectrometer and LECO CS-244 infrared (IR) spectrometer.

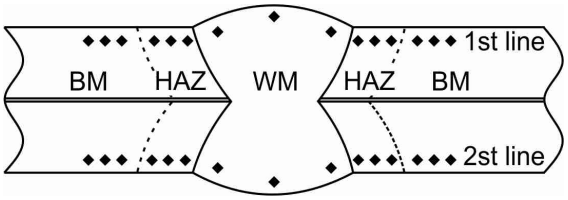

Figure 2. Hardness measurement scheme

3. Results and discussion

3.1 Macro imagery

Macro images of welds are shown in Figures 3 and 4. It should be noted that in all specimens except for specimens 6, 7 and 8 (Figs. 4b, 4c and 4d), a full penetration was achieved. Therefore, in specimens welded with M21, a slightly lower penetration was achieved, which can be influenced by the shielding gas used. Also, the specific feature of these specimens is the presence of polymer interlayer, which evaporates during welding, separating the plates, which can influence the lack of penetration during welding. It can be seen that in all specimens shown in Figures 3 and 4 a common weld metal of a columnar type is present. Also, in specimens with V preparation, a lower and in some cases a non-existent reinforcement can be found. In these specimens, a wider heat-affected zone can be noticed, which can be the result of a lower welding speed. Some weld imperfections were noted in specimens welded (Fig. 4) in form of inclusions (entrapped slag), which can be the result of a lower penetration performed with M21 shielding gas.

3.2 Hardness results

The hardness results (HV 10) are shown in Figure 5. The hardness of the base metal is relatively uniform and in accordance with the tensile strength presented in Table 3. All hardness values obtained in heat affected zone are under 300 HV. It can be seen that in all specimens the WM is harder than the HAZ and base metal, which is the result of a consumable material mixing with the base metal. The consumable material has a higher carbon content and contains alloying elements as well, influencing a higher hardness in the WM. Other hardness values are similar in different areas.

3.3 Tensile and bend testing

Tensile and bend testing results are shown in Table 3. In specimens 1, 2, 3, 4 and 7, the fracture occurred in the base material. In specimens 5 and 6, mixed base material and weld metal fracture occurred, while in specimen 8, weld metal fracture occurred. Generally, specimens welded with C1 shielding gas offer higher tensile strength than specimens welded with M21. It can be seen that the highest tensile strength was obtained in specimen 4, closely followed by specimens 2, 3 and 1. On the other hand, the lowest tensile strength was obtained with specimen 8.

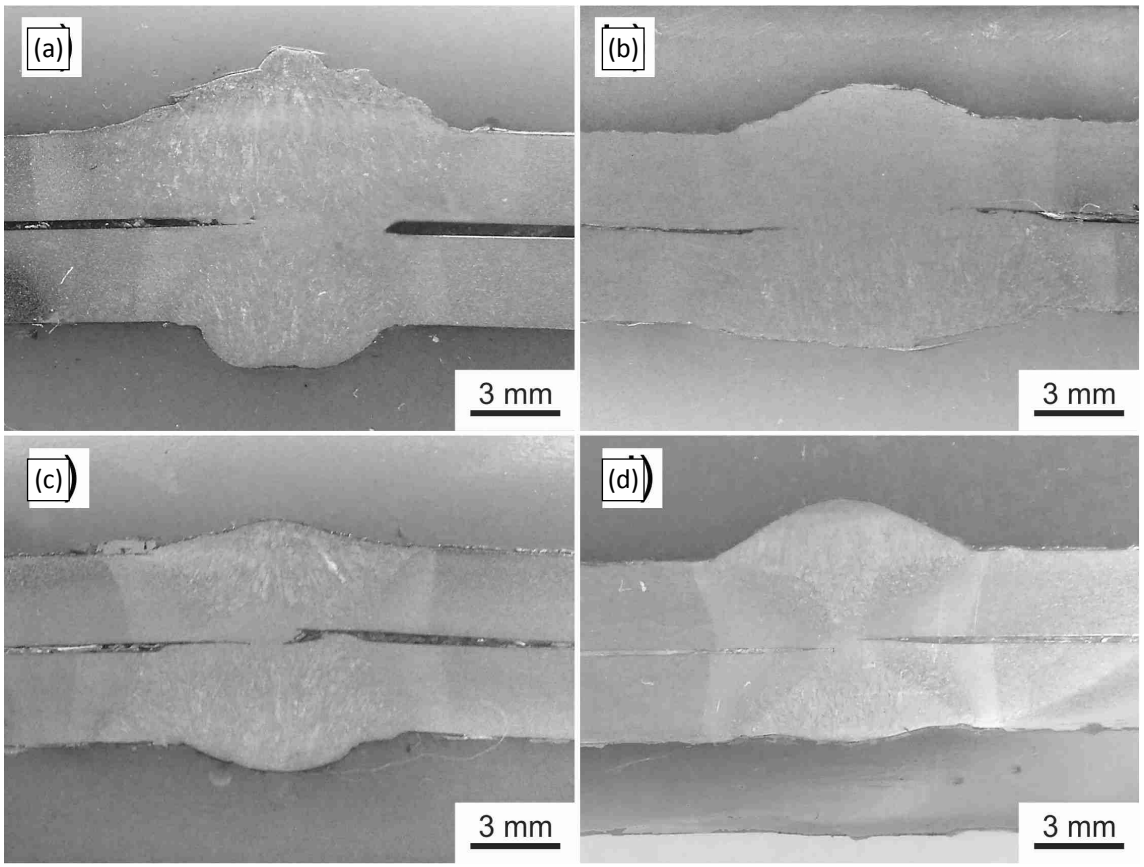

Figure 3. Specimens welded with C1 shielding gas: (a) specimen 1, (b) specimen 2, (c) specimen 3 and (d) specimen 4

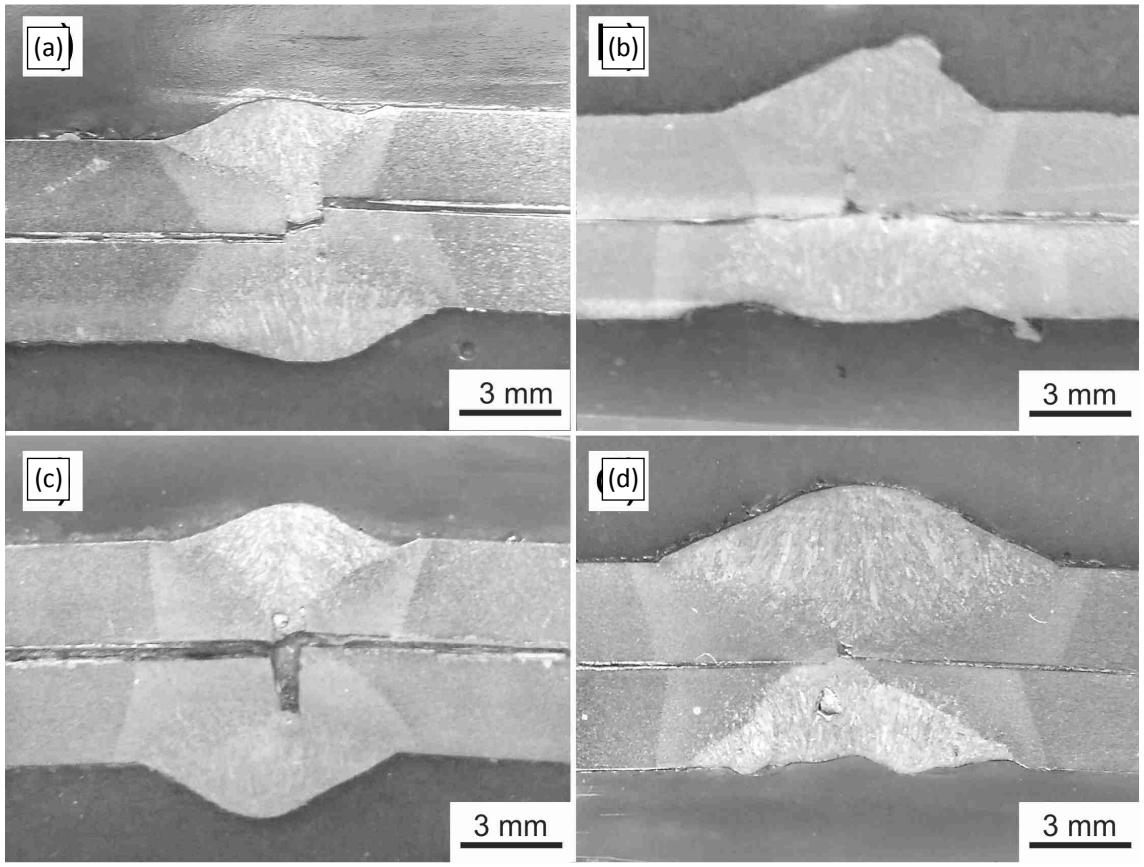

Figure 4. Specimens welded with M21 shielding gas: (a) specimen 5, (b) specimen 6, (c) specimen 7 and (d) specimen 8

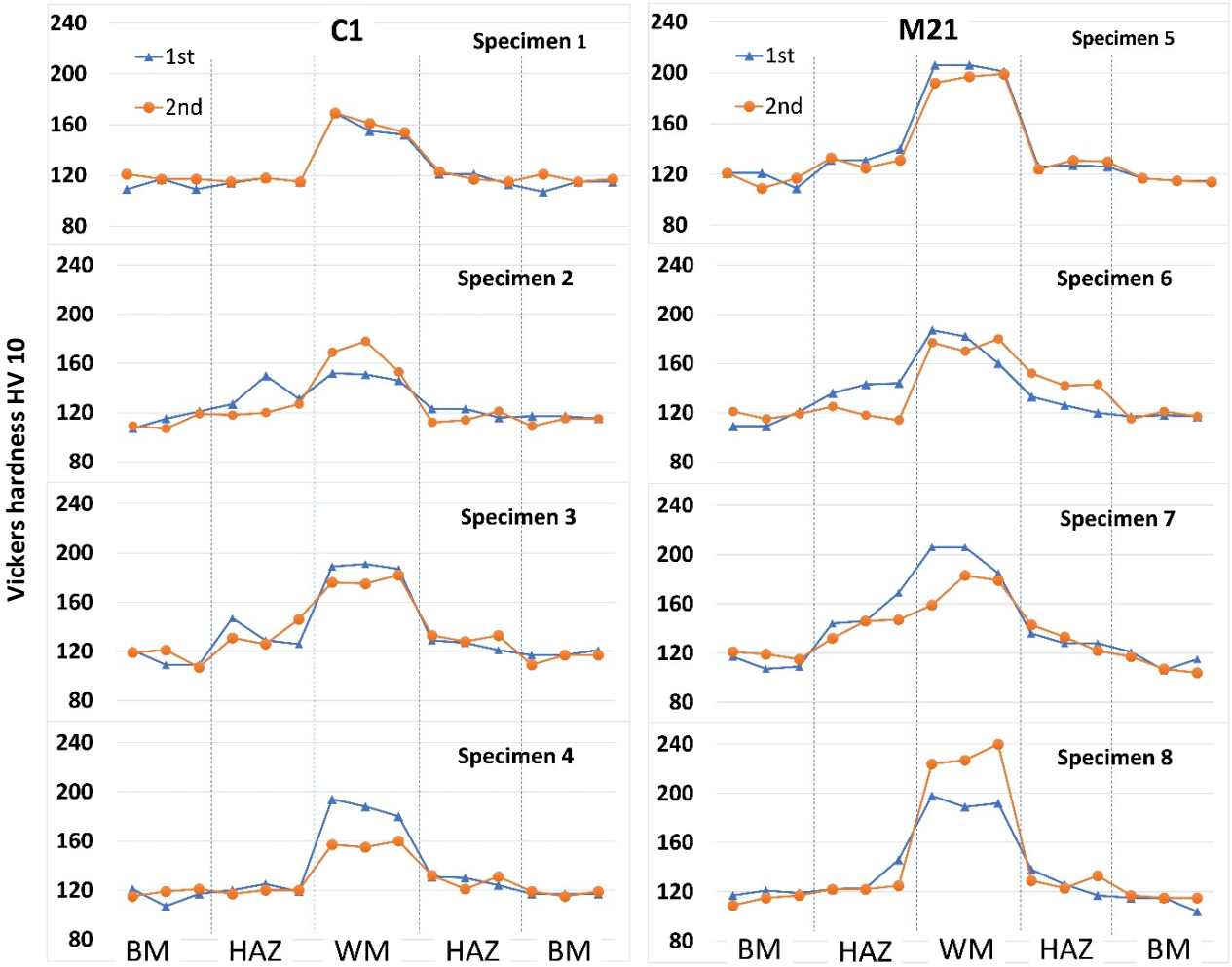

Figure 5. Hardness distributions in specimens welded with C1 and M21 shielding gases

Table 3. Tensile and bend testing results

Specimen	Tensile testing		Bend testing
	Tensile strength, MPa	Place of fracture	
1	287±6	BM, BM, BM	No crack or fracture
2	292±3	BM, BM, BM	No crack or fracture
3	292±3	BM, BM, BM	No crack or fracture
4	294±6	BM, BM, BM	No crack or fracture
5	235±35	BM, BM, WM	Four cracks
6	243±55	BM, WM, BM	No crack or fracture
7	268±11	BM, BM, BM	One crack
8	161±29	WM, WM, WM	Three cracks one fracture

Bend testing revealed that cracks occurred in specimens 5, 7 and 8 (Fig. 6). Furthermore, in specimen 8, three cracks and one fracture occurred during bending. Clearly, C1 as a shielding gas and welding with inverted V preparation proved safer from the point of view of tensile testing and bending, enabling a higher penetration and a full remelting of the material at the joint. On the other hand, M21 shielding gas does not provide full penetration, leaving non-remelted material that already has initial cracks at the edges between the remelted and non-remelted base material.

It was expected that tensile and bend tests are in full correlation. However, it was found that in certain specimens (5 and 7) a discrepancy occurs between tensile and bend test results. This indicates variable weld mechanical properties, related to a probable uneven penetration. On the other hand, the highest combined tensile and bending properties were found in specimens 1, 2, 3 and 4, while the lowest in specimen 8, which can be positively correlated to macro imagery shown in Figures 3 and 4.

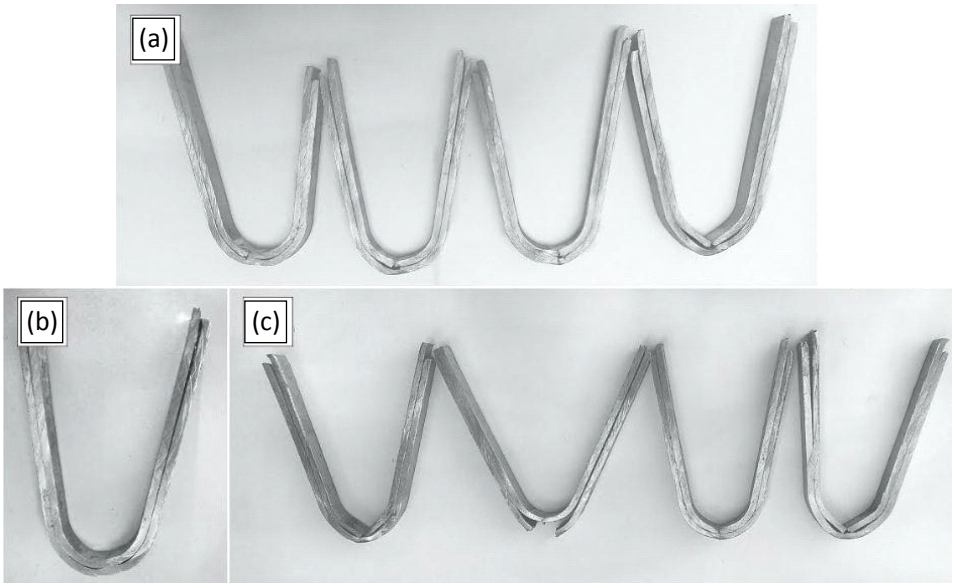

Figure 6. Bend tests with cracks and fractures: (a) specimen 5, (b) specimen 7 and (c) specimen 8

3.4 Microstructural examination

For the purpose of rationality, only the microstructure of specimens 1 and 8 is presented. These two specimens were chosen due to a large discrepancy between their mechanical properties.

In Figures 7 and 8, the microstructures of specimens 1 and 8 are shown, respectively. All microstructures are similar, except for the reheated zone that is not present in specimen 8. Weld metals in the columnar zone (Figs. 7a and 8a) show the microstructure that is consisted of a predominant ferrite with different morphologies. Acicular, Widmanstaetten and allotriomorphic ferrite are present. Weld metal in the reheated zone in specimen 1 (Fig. 7b) shows a refined polygonal ferrite obtained after the second welding pass heat treated the primary microstructure of the first weld pass. Heat affected zone shown in Figures 7c and 8b also consists of polygonal ferrite of a slightly larger grain size compared to the reheated weld metal zone. Finally, the base metal microstructure (Figs. 7d and 8c) consists of elongated ferrite grains as the result of rolling, which was expected and in agreement with the base metal chemical composition, Table 1.

3.5 Chemical composition of welds

Chemical compositions of WM and HAZ of representative specimens 1 and 8 are shown in Tables 4 and 5. Compared to the composition of the base metal shown in the experimental part, it can be seen that C, Si and Mn contents are higher, as the result of alloying elements that come from the consumable wire. The chemical composition of the HAZ is very similar to the base metal, which indicates that the influence of the polymer interlayer is kept at a very low level. Also, there are few differences between these two representative specimens. Cu content in WM is slightly higher in specimen 1, which can be the result of deeper penetration and the analysis done in the remelted area between the steel sheets. The largest difference in WM is in the Si and Mn content which is higher in specimen 8, due to a lower loss of these alloying elements, probably as a result of a lower penetration. As the chemical composition was measured on the inside of the plate, the specimen preparation revealed the surface that was not affected by the inner free surface of the base metal as in specimen 1 with higher penetration.

3.6 Polymer interlayer thicknesses in weld zones

Evaporation, melting and cross-linking areas are shown in Figure 9, while the measured distances in welded specimens are shown in Table 6. Average evaporation distances are the largest, followed by cross-linking distances and finally, degradation distances. In general, evaporation, melting and cross-linking distances in specimens 1, 2, 3 and 4 are larger than in specimens 5, 6, 7 and 8, probably due to the application of C1 shielding gas, in contrast to M21 with a lower oxygen content and the highest. The highest polymer damaged distances from the plate edge were obtained in specimen 2, most probably due to the highest heat input rate, making a clear trade-off for mechanical

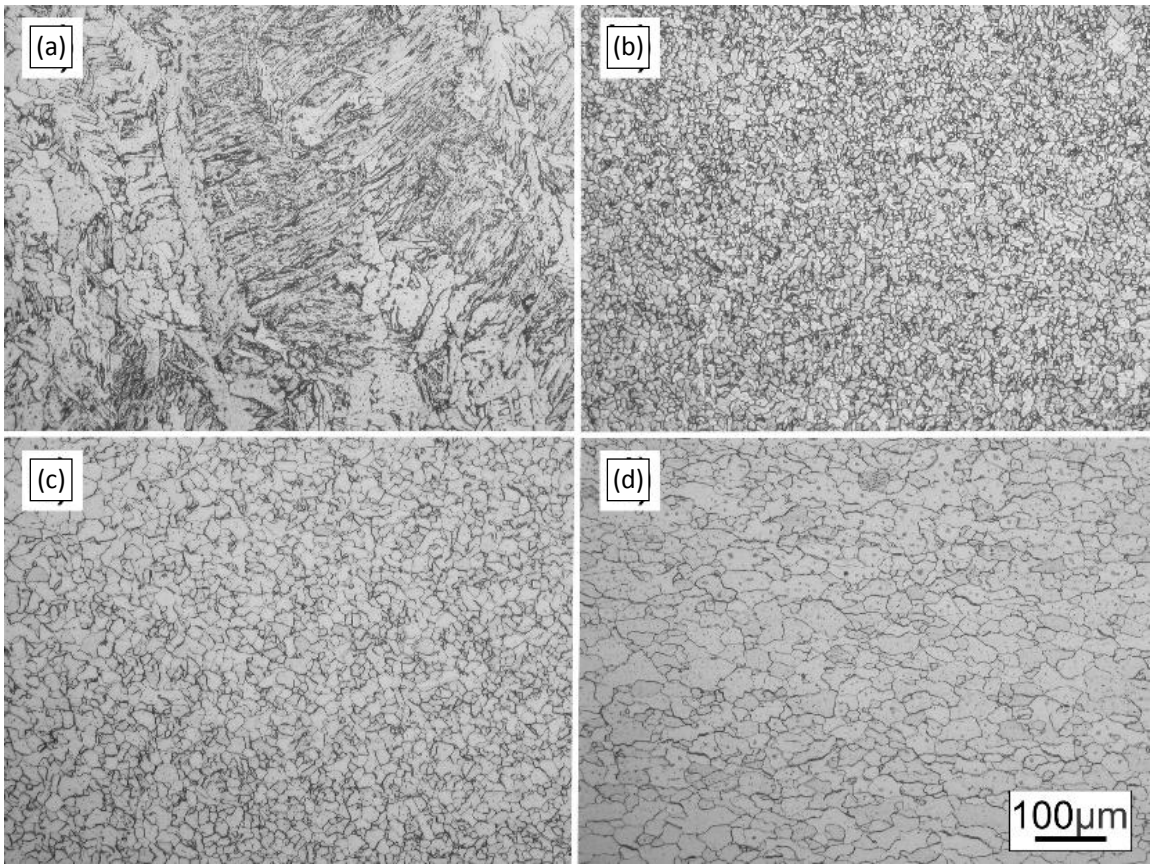

Figure 7. Microstructures of specimen 1: (a) weld metal – columnar zone, (b) weld metal – reheated zone, (c) heat affected zone and (d) base metal

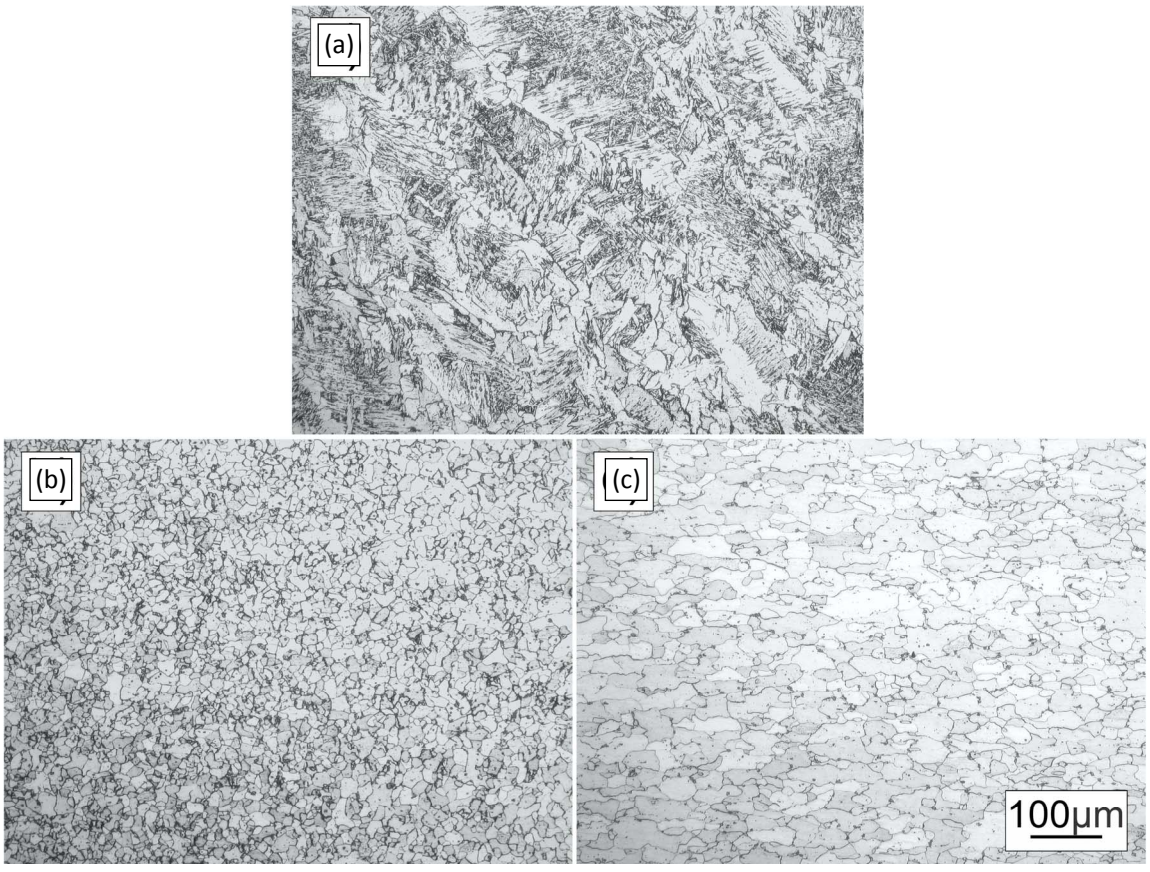

Figure 8. Microstructures of specimen 8: (a) weld metal – columnar zone, (b) heat affected zone and (c) base metal

Table 4. Chemical compositions of WM of specimens 1 and 8 (wt. %)

Specimen	C	Si	Mn	S	Cr	P	Al	Cu	Ni
1	0.09	0.37	0.682	0.007	0.038	0.007	0.011	0.070	0.017
8	0.06	0.41	0.765	0.006	0.038	0.008	0.012	0.067	0.017

Table 5. Chemical compositions of HAZ of specimens 1 and 8 (wt. %)

Specimen	C	Si	Mn	S	Cr	P	Al	Cu	Ni
1	0.04	0.01	0.193	0.005	0.033	0.005	0.037	0.021	0.020
8	0.04	0.01	0.192	0.005	0.039	0.006	0.038	0.021	0.021

Figure 9. Evaporation, melting and cross-linking areas in specimen 4

Table 6. Evaporation, melting and cross-linking distances in welded specimens

Specimen	Evaporation distance (average), mm	Degradation distance (average), mm	Cross-linking distance (average), mm
1	6.5 – 13.2 (9.85)	2.2 – 5.3 (3.75)	5.7 – 7.3 (6.5)
2	7.5 – 15.1 (11.3)	3.8 – 5.3 (4.55)	7.7 – 9.6 (8.65)
3	7.1 – 12.2 (9.65)	2.8 – 4.7 (3.8)	3.6 – 6.8 (5.2)
4	5.3 – 11.8 (8.55)	3.1 – 3.5 (3.3)	5.0 – 8.8 (6.9)
5	4.6 – 8.0 (6.3)	1.6 – 3.0 (2.3)	3.6 – 4.8 (4.2)
6	3.6 – 10.3 (6.95)	4.4 – 6.2 (5.3)	4.6 – 4.7 (4.65)
7	8.0 – 8.2 (8.1)	2.2 – 2.3 (2.25)	4.4 – 5.5 (4.95)
8	4.0 – 5.0 (4.5)	1.8 – 3.2 (2.5)	1.5 – 1.7 (1.6)

properties. The lowest evaporation distance, relevant for fume development was obtained in specimen 8, however, from the point of view of structural strength, this specimen is unacceptable. Obviously, by using a M21 gas, with a lower oxygen content, a lower evaporation distance can be obtained, but at the same time, lower mechanical properties can be obtained.

If the mechanical properties are deemed the most important from the point of structural integrity, the specimens 1, 2, 3 and 4 welded with C1 have a clear advantage over the specimens 5, 6, 7 and 8 welded with M21 shielding gas.

If the simplicity combined with overall welding speed is indicated as a priority, specimen 1 is optimal, interrupting the welding in specimens 3 and 4 also takes time, particularly to establish the arc and to overlap the welds. As characteristic distances are similar in specimens 1 and 3, and specimen 1 is considerably faster to weld as it is welded in one pass on each side, it can be considered as optimal of the specimens tested. If the strength and evaporation distance are indicated as most important, then specimen 4 is optimal, at the cost of fabrication time.

4. Conclusions

Within the limitations of the experiment, the following conclusions can be drawn:

- A reliable full penetration was achieved in specimens 1, 2, 3 and 4, welded with C1 shielding gas.
- The highest tensile strength and the most convenient bending properties were obtained with specimens 1, 2, 3 and 4. This is understandable due to a full penetration obtained in these specimens.
- Specimens 5, 6, 7 and 8, although their evaporation distance is lower compared to specimens 1, 2, 3 and 4, the lack of penetration causes the resulting carbon to migrate into the heat affected zone and weld metal, increasing the local hardness.
- Specimens welded with M21 shielding gas have lower tensile properties, indicating the lowest structural integrity of the housing. Lower tensile properties are the result of lower penetration and inclusions in form of slag entrapment.

The specimen welded in one pass (specimen 1) on each side was judged to be the optimal combination of mechanical strength and technological simplicity and speed of preparation and welding. The minimal evaporation distance at acceptable mechanical properties was obtained in specimen 4.

Acknowledgement

The authors gratefully acknowledge research support by the project entitled “Materials, joining and allied technologies” on the Department of Production Engineering, Faculty of Technical Sciences Novi Sad, Serbia.

References

[1] M. Harhash, H. Palkowski, Incremental sheet forming of steel/polymer/steel sandwich composites, Journal of Materials Research and Technology, Vol. 13, 2021, pp. 417-430, DOI: 10.1016/j.jmrt.2021.04.088

[2] I. Burchitz, R. Boesenkool, S. van der Zwaag, M. Tassoul, Highlights of designing with Hylite – A new material concept, Materials & Design, Vol. 26, No. 4, 2005, pp. 271-279, DOI: 10.1016/j.matdes.2004.06.021

[3] Springer Fachmedien Wiesbaden, Einsatzpotenzial von Litecor in der karosserie [Application Potential of Litecor in the Body], ATZ extra, Vol. 19, No. 10, 2014, pp. 108-111, DOI: 10.1365/s35778-014-1338-x [in German].

[4] T.M. Link, Formability and performance of steel-plastic-steel laminated sheet materials, SAE Technical Paper Series, 2001, Paper 2001-01-0079, DOI: 10.4271/2001-01-0079

[5] S. Wiedemann, H. Wessels, H.-J. Wetterau, L. Eckstein, T. Schulte, N. Modler, J. Jaschinski, T. Weber, T. Wollmann, R. Kawalla, C. Krbetschek, M. Oswald, M. Ullmann, F. Berge, N.B. Khalifa, M. Hahn, R. Schwarzer, B. Poggel, M. Würtele, … B. Lehmhaus, LEIKA: Effiziente Mischbauweisen für Leichtbau-Karosserien, Plattform FOREL, Dresden, 2017 [in German].

[6] M. Gude, K. Demnitz, M. Müller, M. Stegelmann, G. Meschut, M. Gerkens, J. Göddecke, D. Han, M.F. Zäh, A. Hofer, A. Schönmann, S. Schreiber, H. Lieberwirth, T. Krampitz, A.E. Tekkaya, M. Hahn, S. Gies, FOREL-Studie 2018: Ressourceneffizienter Leichtbau für die Mobilität, Plattform FOREL, Dresden, 2018 [in German].

[7] R.E. Smallman, A.H.W. Ngan, Physical Metallurgy and Advanced Materials, Butterworth-Heinemann, Oxford, 2007.

[8] S. Balos, L. Sidjanin, B. Sabo, V. Grabulov, Tehnologija zavarivanja polimetilmetakrilata (PMMA) [Polymethylmethacrylate (PMMA) welding technology], Zavarivanje i zavarene konstrukcije, Vol. 55, No. 4, 2010, pp. 143-146 [in Serbian].

[9] Antiphon MPM – Structure-borne damping sheet metal laminate, available at: https://antiphon.se/en/products-and-applications/mpm-structure-borne-sound-damping-laminate, accessed: 13.04.2022.

[10] Pyrotec – Soundsteel / sound alloy, available at: https://www.pyroteknc.com/dmsdocument/140/Soundmetal-Install-101-1IG.pdf, accessed: 15.04.2022.

[11] I. Hrivnjak, Zavarljivost čelika, IRO Građevinska knjiga, Belgrade, 1982 [in Serbian].

[12] V. Palić, Zavarivanje, Fakultet tehničkih nauka, Novi Sad, 1987 [in Serbian].

[13] Böhler welding – Welding guide, available at: http://www.bohlerwelding.ru/files/cat/full_catalog.pdf, accessed: 18.04.2022.